Journal of Molecular Cell Biology (2023), 15(1), mjad001 https://doi.org/10.1093/jmcb/mjad001
Published online January 10, 2023

Article

RIG-I immunotherapy overcomes radioresistance in p53-positive malignant melanoma

Silke Lambing[1], Yu Pan Tan[1], Paraskevi Vasileiadou[1], Stefan Holdenrieder[1,2], Patrick Müller[1], Christian Hagen[1], Stephan Garbe[3], Rayk Behrendt[1], Martin Schlee[1], Jasper G. van den Boorn[1], Eva Bartok[1,4,5,†,*], Marcel Renn[1,6,†], and Gunther Hartmann[1,†,*]

[1] Institute of Clinical Chemistry and Clinical Pharmacology, University Hospital Bonn, Bonn 53127, Germany
[2] Institute of Laboratory Medicine, German Heart Centre, Munich 80636, Germany
[3] Department of Radiation Oncology, University Hospital Bonn, Bonn 53127, Germany
[4] Unit of Experimental Immunology, Department of Biomedical Sciences, Institute of Tropical Medicine, Antwerp 2000, Belgium
[5] Institute of Experimental Haematology and Transfusion Medicine, University Hospital Bonn, Bonn 53127, Germany
[6] Mildred Scheel School of Oncology, Bonn, University Hospital Bonn, Medical Faculty, Bonn 53127, Germany
[†] These authors contributed equally to this work.
* Correspondence to: Eva Bartok, E-mail: ebartok@uni-bonn.de; Gunther Hartmann, E-mail: gunther.hartmann@uni-bonn.de

Edited by Hua Lu

Radiotherapy induces DNA damage, resulting in cell cycle arrest and activation of cell-intrinsic death pathways. However, the radioresistance of some tumour entities such as malignant melanoma limits its clinical application. The innate immune sensing receptor retinoic acid-inducible gene I (RIG-I) is ubiquitously expressed and upon activation triggers an immunogenic form of cell death in a variety of tumour cell types including melanoma. To date, the potential of RIG-I ligands to overcome radioresistance of tumour cells has not been investigated. Here, we demonstrate that RIG-I activation enhanced the extent and immunogenicity of irradiation-induced tumour cell death in human and murine melanoma cells *in vitro* and improved survival in the murine B16 melanoma model *in vivo*. Transcriptome analysis pointed to a central role for p53, which was confirmed using p53$^{-/-}$ B16 cells. *In vivo,* the additional effect of RIG-I in combination with irradiation on tumour growth was absent in mice carrying p53$^{-/-}$ B16 tumours, while the antitumoural response to RIG-I stimulation alone was maintained. Our results identify p53 as a pivotal checkpoint that is triggered by RIG-I resulting in enhanced irradiation-induced tumour cell death. Thus, the combined administration of RIG-I ligands and radiotherapy is a promising approach to treating radioresistant tumours with a functional p53 pathway, such as melanoma.

Keywords: RIG-I, p53, melanoma, immunotherapy, irradiation, radiotherapy, radioresistance

Introduction

Radiation therapy is a mainstay of antitumour therapy for lymphoma, breast, brain, as well as head and neck cancers. It is currently used in the treatment schedule of 50% of all malignancies (Delaney and Barton, 2015). Since radiotherapy has been demonstrated not only to restrict tumour cell proliferation but also to induce tumour-specific CD8$^+$ T cells (Lee et al., 2009), it is also studied in combination with tumour immunotherapies, such as checkpoint inhibitors, in preclinical and clinical trials (Kang et al., 2016). Irradiated tumour cells release pro-inflammatory cytokines, including (i) chemokine (C–X–C motif) ligand 16 (CXCL16) and tumour necrosis factor α (TNFα) (Hallahan et al., 1989; Matsumura et al., 2008), (ii) the ligand of STING—cyclic guanosine monophosphate–adenosine monophosphate (Marcus et al., 2018; Schadt et al., 2019), and (iii) alarmins such as high mobility group box 1 (HMGB1) and adenosine triphosphate (Apetoh et al., 2007; Ohshima et al., 2010; Golden et al., 2014). There are also reports that ionizing radiation can induce the expression of major histocompatibility complex class I (MHC-I) proteins (Hauser et al., 1993; Reits et al., 2006) and calreticulin (Obeid et al., 2007a; Gameiro et al., 2014) on the surface of irradiated, dying cells, which promotes recognition and internalization of the cells by phagocytes and

Received March 13, 2022. Revised September 25, 2022. Accepted January 9, 2023.

subsequent T cell activation. However, many tumours, such as malignant melanoma, are primarily radioresistant or develop radioresistance upon repeated radiotherapy (Mahadevan et al., 2015; van den Berg et al., 2020), limiting the utility of this approach.

Recent advances in immunotherapy have significantly prolonged survival for patients with many different tumour entities (Esfahani et al., 2020). While immune checkpoint inhibition is effective in a portion of patients, the presence of an anti-inflammatory (cold) tumour microenvironment and lack of pre-existing tumour-antigen-specific T cells still pose strong limitations for checkpoint-inhibitor treatment in many patients (Bonaventura et al., 2019). One promising approach for 'converting' the tumour microenvironment to make it amenable to immune-cell infiltration and to mount an effective antitumour response is the targeted stimulation of innate immune receptors, including the cytosolic, antiviral receptor retinoic acid-inducible gene I (RIG-I). RIG-I is broadly expressed in nucleated cells, including tumour cells, and can be specifically activated by 5′-tri- or 5′-diphosphorylated, blunt-ended, double-stranded RNA (dsRNA) (Hornung et al., 2006; Schlee et al., 2009; Goubau et al., 2014). RIG-I activation leads to the induction of type I interferon (IFN) and pro-inflammatory cytokines (Hornung et al., 2006; Schlee et al., 2009; Goubau et al., 2014). Moreover, it directly induces tumour cell death (Poeck et al., 2008; Besch et al., 2009) with classical 'immunogenic' hallmarks, such as HMGB1 release and calreticulin exposure on the cell surface (Duewell et al., 2014; Bek et al., 2019; Castiello et al., 2019). Intratumoural activation of RIG-I exhibits features of a cancer vaccine by simultaneously inducing the release of tumour antigens and creating a pro-immunogenic environment that facilitates the development of tumour-specific cytotoxic T cells (van den Boorn and Hartmann, 2013; Bek et al., 2019).

We hypothesized that the combination of irradiation and specific RIG-I activation changes the tumour microenvironment to become 'hot', thus enabling an effective antitumour response. Here, we studied the combination of a synthetic RIG-I-specific ligand, 5′-triphosphate dsRNA (3pRNA), with irradiation. We found in both human and murine melanoma cell lines that the combination of RIG-I activation and irradiation significantly increased immunogenic tumour cell death and improved the uptake of dead tumour cells by dendritic cells (DCs) and their subsequent activation. The analysis of transcriptomic data identified a critical role for the p53 pathway, which was confirmed by using $p53^{-/-}$ B16 cells. While the antitumour effects of RIG-I monotherapy were independent of p53, the RIG-I-mediated increase in the susceptibility of tumour cells to irradiation was found to be p53-dependent. Cotreatment of 3pRNA with tumour-targeted irradiation enhanced the activation of T cells and natural killer (NK) cells in draining lymph nodes and prolonged the overall survival of tumour-bearing animals in an *in vivo* B16 melanoma model. Altogether, our study suggests that combined radiotherapy–RIG-I immunotherapy has great clinical potential, especially in patients with radioresistant tumours exhibiting an intact p53 pathway, like most malignant melanomas.

Results

Combined radiotherapy–RIG-I immunotherapy induces immunogenic tumour cell death, improves tumour cell uptake by DCs, and activates DCs in vitro

To investigate whether RIG-I activation combined with irradiation had a synergistic effect on the induction of immunogenic cell death *in vitro*, we stimulated the murine B16 and human A375 melanoma cell lines with the RIG-I ligand 3pRNA followed by 2 Gy of irradiation. RIG-I synergistically increased the irradiation-induced cell death, as measured by Annexin V/7-amino-actinomycin D (7AAD) staining; notably, this effect could not be recapitulated by the addition of recombinant IFNα to 2 Gy-irradiated cells (Figure 1A and B; Supplementary Figure S1A and B). The synergistic effect was confirmed by calculating the combination index. Increased induction of cell death was confirmed by examining intracellular levels of cleaved caspase 3 (Supplementary Figure S1C). Moreover, RIG-I activation and irradiation significantly lowered the EC_{50} of 3pRNA for the induction of cell death, from 987 ng/ml 3pRNA alone to 293 ng/ml 3pRNA in combination with 2 Gy radiation in murine B16 cells and from 1754 ng/ml to 333 ng/ml in human A375 melanoma cells (Figure 1C and D; Supplementary Figure S1D and E). Since RIG-I stimulation by 3pRNA showed the greatest synergistic effect on cell death induced by 2 Gy irradiation (Supplementary Figure S1F), this irradiation dose was selected for all subsequent experiments to analyze the effect of the combination therapy. In addition to A375, several other human melanoma cell lines (MaMel19, MaMel54, and MaMel48) and A549 lung adenocarcinoma cells were tested, which also showed increased cell death when RIG-I stimulation was combined with irradiation (Figure 1E and F).

Calreticulin exposure on the outer leaflet of the cell membrane induces the efferocytosis of dead or dying cells by antigen-presenting cells and is a hallmark of immunogenic cell death (Obeid et al., 2007b). In agreement with the increased Annexin V staining, calreticulin exposure was also found significantly increased upon combined irradiation and RIG-I activation in murine B16 melanoma cells and human A375 cells (Figure 1G and H). Surface expression of calreticulin was highest in Annexin V/7AAD double-positive cells, which are known at the late stage of programmed cell death (Supplementary Figure S1G). Interestingly, the expression of MHC-I on murine B16 cells and human A375 cells was also strongly induced by the combination treatment, most prominently on Annexin V/7AAD-negative cells (Supplementary Figure S1G–I). Furthermore, enzyme-linked immunosorbent assay (ELISA) data showed that the release of the nuclear protein HMGB1, which serves as a danger-associated molecular pattern and is characteristic of immunogenic cell death, was induced by RIG-I stimulation in both cell lines and further increased by 2 Gy irradiation in human A375 cells (Figure 1I and J). RIG-I stimulation, but not 2 Gy irradiation, induced the release of type I IFN in murine B16 cells and type I/III IFN in human A375 cells. In murine B16 cells, combination treatment slightly enhanced the secretion of interleukin 6 (IL6) and TNFα

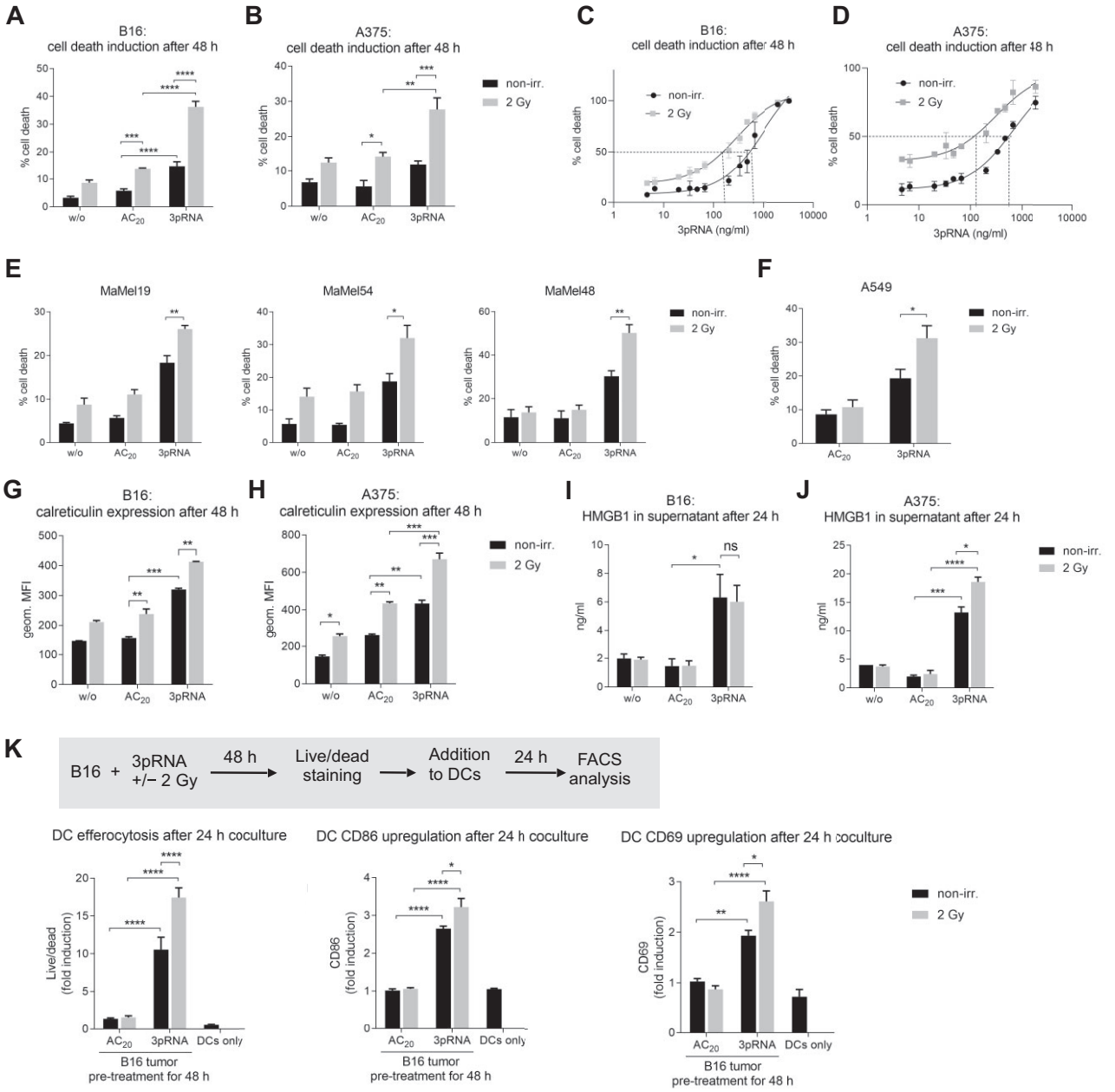

Figure 1 Irradiation enhances 3pRNA-induced immunogenic cell death in melanoma cells, uptake of dead tumour cells by DCs, and activation of DCs. (**A**–**D**) Murine B16 and human A375 melanoma cells were transfected with 50 ng/ml 3pRNA or AC_{20} control RNA followed by 2 Gy irradiation. After 48 h, apoptosis was measured in B16 (**A** and **C**) and A375 (**B** and **D**) cells using Annexin V/7AAD detection by flow cytometry. The dose of 3pRNA ligand was titrated in B16 (**C**) and A375 (**D**) cells to determine the EC50 values with and without 2 Gy irradiation. (**E** and **F**) Different human melanoma cell lines were transfected with 50 ng/ml (MaMel19) or 200 ng/ml (MaMel54 or MaMel48) 3pRNA and irradiated (2 Gy) where indicated. Human lung carcinoma cell line A549 was transfected with 50 ng/ml 3pRNA and irradiated (2 Gy) where indicated. Induction of cell death was quantified 48 h later using Annexin V/7AAD staining and flow cytometry. (**G**–**J**) Melanoma cells were transfected with 50 ng/ml 3pRNA and irradiated (2 Gy). The expression level of calreticulin on the cell surface at 48 h after transfection was measured by flow cytometry (**G** and **H**); HMGB1 concentration in the supernatant at 24 h after transfection was measured by ELISA (**I** and **J**). (**K**) B16 cells were treated with 200 ng/ml 3pRNA and 2 Gy irradiation, and after 48 h, stained with fixable viability dye, and then cocultured with BMDCs from wildtype C57BL/6 mice for 24 h. Uptake of tumour cells by DCs and activation of DCs were measured by flow cytometry. Percentage of cell death was plotted as the sum of Annexin V-positive, Annexin V/7AAD double-positive, and 7AAD-positive populations divided by the total number of cells. **A**, **B**, **E**, **F**, and **K**: data are shown as mean ± SEM ($n = 3$); **I** and **J**: $n = 2$ independent experiments; **C**, **D**, **G**, and **H**: representative results shown as mean ± SD of $n = 3$ independent experiments with similar results. *$P < 0.05$; **$P < 0.01$; ***$P < 0.001$; ****$P < 0.0001$; two-way ANOVA. geom. MFI, geometric mean fluorescence intensity; w/o, untreated; non-irr., non-irradiated.

but did not increase the release of IFN or IFN-stimulated CXCL10 (Supplementary Figure S2A), whereas in human A375 cells, IL6, granulocyte-macrophage colony-stimulating factor, IL29 (IFNλ1), and CXCL10, but not IFNβ, were enhanced by irradiation with RIG-I stimulation (Supplementary Figure S2B).

To test whether the combination treatment had an impact on tumour cell uptake by professional antigen-presenting cells and their activation, B16 melanoma cells were treated with 3pRNA and irradiation, and then stained with eFluor780 fixable viability dye and co-incubated with bone marrow-derived DCs (BMDCs). BMDCs 'fed' with B16 cells after combination treatment demonstrated higher levels of eFluor780 dye uptake compared with those 'fed' with B16 cells after irradiation or RIG-I activation alone (Figure 1K). Combination treatment also significantly enhanced the expression of the costimulatory molecule CD86 and the immune-cell activation marker CD69 (Figure 1K).

Radiotherapy–RIG-I immunotherapy prolongs the survival of B16 melanoma-bearing mice in vivo

Next, we studied the effet of combined irradiation and RIG-I activation *in vivo*. C57BL/6 mice with a palpable subcutaneous B16 melanoma were treated with 2 Gy precision irradiation of the tumour area and intratumoural injection of 20 μg 3pRNA or 20 μg of non-stimulatory polyA control RNA twice a week. Compared with untreated groups, 3pRNA treatment alone and treatment with irradiation combining control RNA or 3pRNA prolonged the survival of the mice, and the combination treatment of irradiation and 3pRNA resulted in the longest overall survival (Figure 2A). Tumour-draining lymph nodes were harvested at 16 h after treatment and analyzed for the expression of the activation marker CD69. In NK cells and $CD8^+$ T cells, CD69 was upregulated upon RIG-I activation, with the highest expression induced by RIG-I activation combined with irradiation, while in $CD4^+$ T cells, only the combination treatment of RIG-I activation and irradiation induced significant upregulation of CD69 (Figure 2B).

Transcriptomic analysis of melanoma cells after combination therapy reveals activation of the p53 signalling pathway

To explore the potential molecular mechanisms of the combination therapy, we performed whole-genome transcriptional analysis with an Affymetrix gene chip on B16 cells at 6 h after treatment with 3pRNA and irradiation. RIG-I stimulation induced a strong change in gene-expression patterns and a robust induction of interferon-stimulated genes (ISGs), whereas irradiation alone primarily induced genes associated with DNA damage response (Figure 3A). As expected, pathway analysis of differentially expressed genes showed that RIG-I stimulation was associated with pathways involved in innate immunity, while irradiation induced genes of the p53 pathway. The p53 pathway was also among the most significantly upregulated pathways in the combination group (Figure 3B). It was the only differentially regulated pathway between the combination group and 3pRNA alone group (Figure 3C and D). Given the central role of p53 signalling in DNA damage and cell cycle control, we reasoned that this pathway may be involved in the observed antitumoural effects of the combination treatment.

Combined irradiation and RIG-I activation cooperatively induce p53 signalling and prolong cell cycle arrest

We then examined the effects of RIG-I activation, irradiation, and combination treatment on p53 phosphorylation and signalling. As expected, 2 Gy irradiation induced p53 phosphorylation at 6 h after treatment, which then declined after 24 h (Figure 4A). In contrast, 3pRNA alone only led to weak p53 phosphorylation after 24 h. However, B16 cells receiving combination treatment with 3pRNA and irradiation retained strong p53 phosphorylation even at 24 h after treatment (Figure 4A). Notably, total p53 protein levels at 24 h were only elevated in 3pRNA-transfected B16 cells (with or without irradiation). Moreover, irradiation combined with control RNA or IFNα did not show these effects. These results confirmed RIG-I as a well-established ISG, which in our study was upregulated in response to RIG-I ligand-mediated stimulation but not to irradiation. Furthermore, irradiation did not enhance RIG-I expression induced by the RIG-I ligand (Supplementary Figure S3A–C). Therefore, irradiation did not enhance RIG-I-induced signalling by further upregulating RIG-I expression.

We then analyzed the expression of two target proteins induced by p53, the proapoptotic p53-upregulated modulator of apoptosis (PUMA) and the cell cycle inhibitor p21, at 24 h after treatment (Figure 4B). PUMA and p21 were induced by RIG-I activation and irradiation, with the strongest signal in the combination group, showing that the effects on p53 stability and phosphorylation (Figure 4A) translate into increased expression of downstream effector molecules (Figure 4B).

To monitor the effects on cell cycle progression, we stained B16 melanoma cells with propidium iodide at 6, 12, and 24 h after 2 Gy irradiation and RIG-I stimulation. Irradiation induced a G2/M cell cycle arrest after 6 h, which was less pronounced after 12 h and completely resolved at 24 h post-irradiation (Figure 4C). RIG-I stimulation alone, on the other hand, led to a G1/S arrest after 24 h, in line with its slower induction of p53 phosphorylation (Figure 4A). The combination of irradiation and RIG-I stimulation led to a G2/M arrest after 6 h, which was maintained even after 24 h (Figure 4C), consistent with the time course for p53 phosphorylation (Figure 4A).

It has been reported that DNA methylation inhibitors, such as 5-Azacytidine (5-AZA) and Decitabine, induce endogenous dsRNA in the context of demethylation of endogenous retroviral elements, thereby inducing RIG-I-like receptor expression and activating downstream signalling (Chiappinelli et al., 2015; Roulois et al., 2015). Therefore, we were interested in whether RIG-I ligand stimulation could be replaced by exposure of tumour cells to 5-AZA or Decitabine. We found that both 5-AZA and Decitabine consistently upregulated p53, induced phosphorylation of p53, and induced cell death in melanoma cells, but irradiation did not enhance this effect. Furthermore, there was

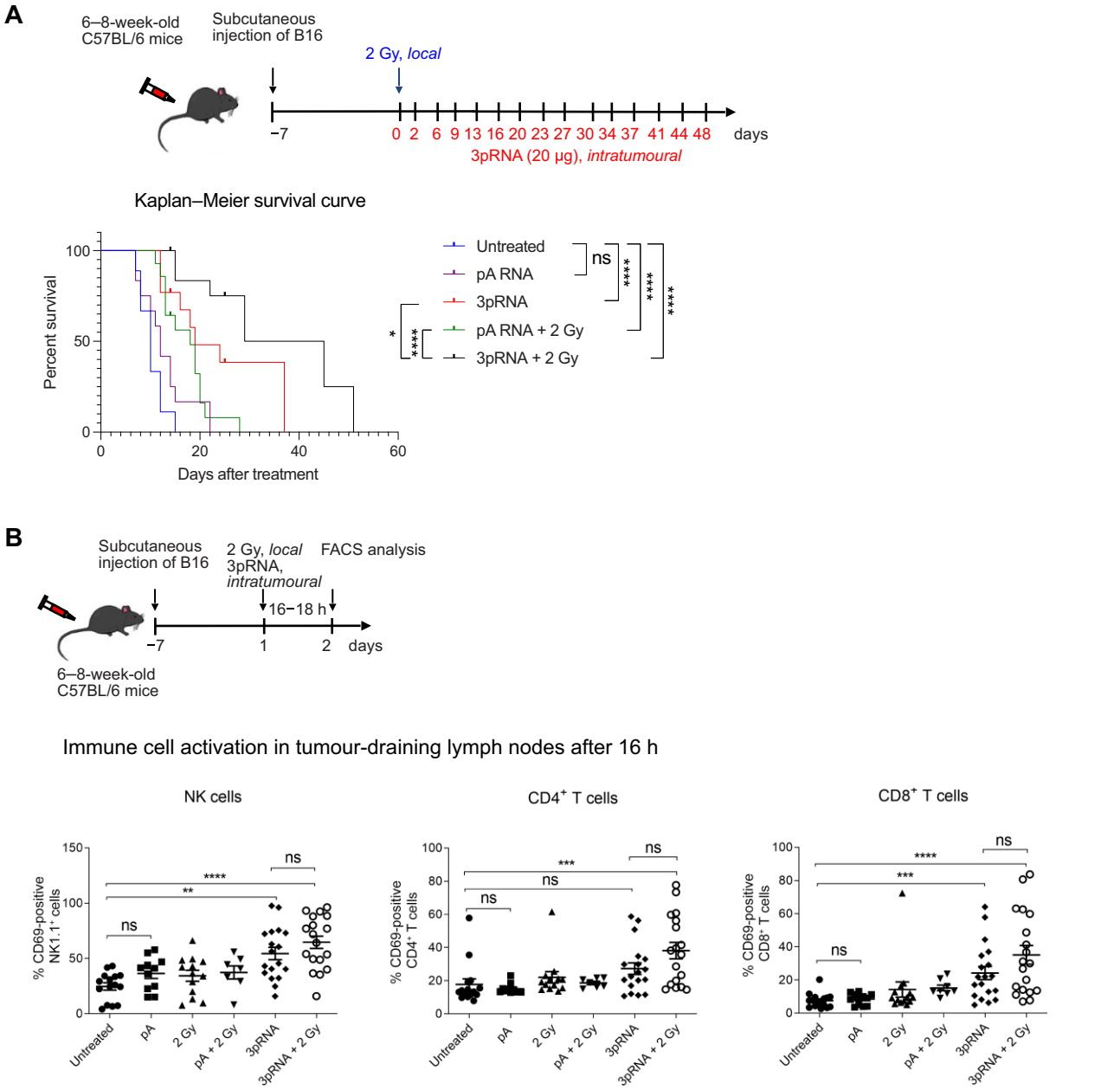

Figure 2 Concurrent irradiation and RIG-I immunotherapy prolong the survival of melanoma-bearing mice. (**A**) C57/BL6 mice were subcutaneously transplanted with B16 melanoma cells, locally irradiated (2 Gy), and injected with 20 µg 3pRNA or 20 µg control RNA (pA) as indicated. Tumour size was measured regularly over 49 days. Mice with tumours >10 mm in diameter were euthanized for ethical reasons. Survival rate is shown as a Kaplan–Meier curve summarizing three independent experiments with 3–5 mice per group and experiment. Mantel–Cox test. (**B**) Mice subcutaneously transplanted with B16 cells were treated as indicated. Approximately 16 h later, immune cells from the tumour-draining lymph nodes were analyzed for the activation marker CD69. Mean ± SEM of $n = 3$ with 3–5 mice per group and experiment. Kruskal–Wallis test. ns, not significant; $^{**}P < 0.01$; $^{***}P < 0.001$; $^{****}P < 0.0001$.

no upregulation of RIG-I expression (Supplementary Figure S4). Since RIG-I was originally identified as a gene induced by retinoic acid in a promyelocytic leukaemia cell line (Sun, 1997; Gene Bank accession number AF038963), we tested the effect of all-trans retinoic acid (ATRA) in B16 melanoma cells. Neither upregulation of RIG-I nor cell death induction was observed by ATRA alone or in combination with irradiation (Supplementary Figure S4).

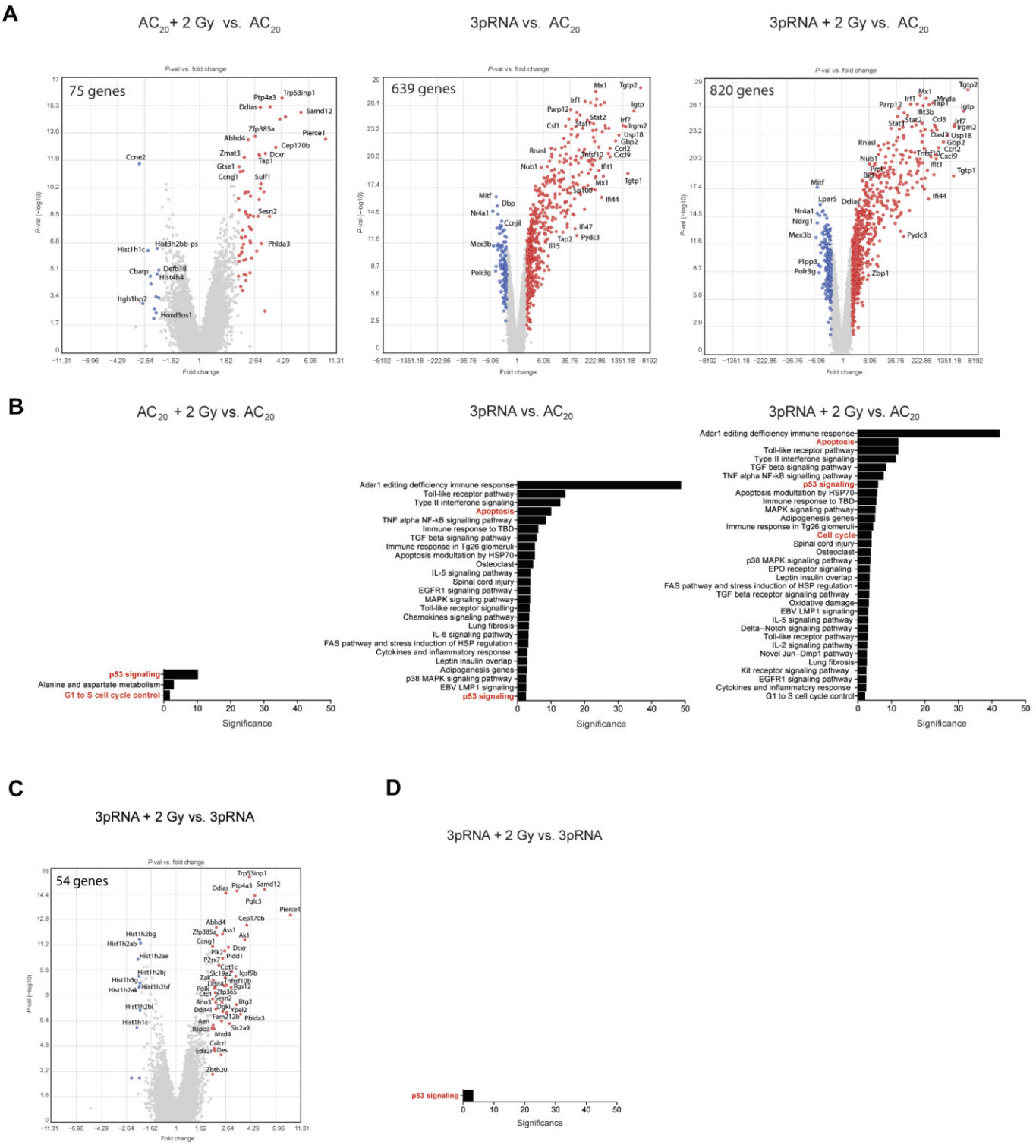

Figure 3 Whole-genome transcriptional analysis of B16 cells treated with combined radiotherapy–RIG-I immunotherapy reveals activation of p53 signalling. (**A** and **C**) Gene-expression analysis (Affymetrix GeneChip) of total RNA from B16 cells at 6 h after stimulation with 50 ng/ml 3pRNA or AC_{20} control RNA, alone or in combination with 2 Gy irradiation. Volcano plots of single and combination treatments in comparison to the control (**A**) and combination treatment vs. 3pRNA treatment (**C**). Coloured data points show upregulation (red) or downregulation (blue) of at least 2-fold change. False discovery rate-corrected *P*-value < 0.05. (**B** and **D**) Pathway analysis (Wikipath) of genes found in **A** and **C**, respectively, using the TAC software of Thermo Fisher ordered by significance.

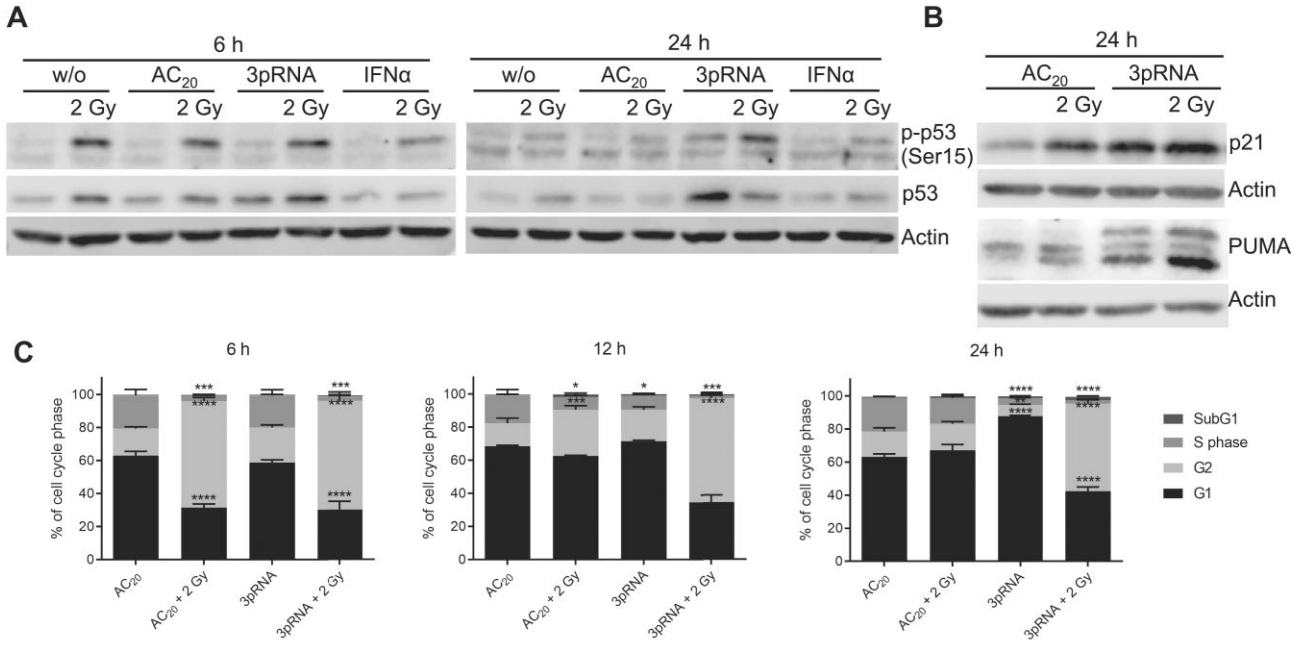

Figure 4 Combined radiotherapy–RIG-I immunotherapy induces p53 pathway activation and prolongs cell cycle arrest. (**A** and **B**) Western blot analysis of phospho-p53 (Ser15), total p53, p21, and PUMA expression after irradiation (2 Gy), transfection of 50 ng/ml 3pRNA, or both in B16 cells at the indicated time points. Actin served as a protein-loading control. (**C**) Flow-cytometric cell cycle analysis of B16 cells stained with propidium iodide at the indicated time points. Mean ± SEM of $n = 2$. ns, not significant; *$P < 0.05$; **$P < 0.01$; ***$P < 0.001$; ****$P < 0.0001$; two-way ANOVA.

Synergistic effect of irradiation and RIG-I activation is p53-dependent, while the effect of RIG-I stimulation alone is p53-independent

To test the functional relevance of p53 in combination therapy, we generated polyclonal p53-knockout ($p53^{-/-}$) cells using CRISPR/Cas9 genome editing. $p53^{-/-}$ B16 and A375 melanoma cells did not show basal p53 expression and, as expected, irradiation did not upregulate p53 protein at 2 h or the p53 target protein p21 at 24 h (Supplementary Figure S5A–D). While the proportions of cell death induced by 3pRNA alone were similar in wildtype and knockout cells, the additional increase of cell death upon irradiation was much more significant in wildtype cells than in $p53^{-/-}$ cells (Figure 5A and B). In contrast to A375 cells carrying wildtype p53 (Supplementary Figure S5E, left panel), human p53-deficient SKmel28 melanoma cells, which carry an endogenous inactivating p53 mutation (Haluska et al., 2006), did not show cell death induced by irradiation. Nevertheless, despite the lack of functional p53, significant cell death was induced by 3pRNA in SKmel28 cells (Supplementary Figure S5E, right panel). Similarly, in $p53^{-/-}$ B16 melanoma cells, RIG-I stimulation alone still induced a G1/S arrest after 24 h and irradiation still induced a G2/M arrest after 6 h, but combination treatment did not induce the prolonged G2/M arrest for 24 and 48 h as observed in wildtype cells (Figure 5C).

Analysis of caspase 3-positive cells in the individual phases of the cell cycle (G1, S, and G2) showed that nearly all of the wildtype cells in the G2 phase underwent cell death and 60% of total wildtype cells were caspase 3-positive at 48 h after combination treatment (Supplementary Figure S6), confirming the results from Annexin V/7AAD staining (Figure 5A) and underscoring the close link between cell cycle arrest and cell death. Accordingly, in the absence of p53, additional irradiation did not show a synergistic effect on cell death (Supplementary Figure S6). Moreover, the proportion of caspase 3-positive cells in each phase of the cell cycle was substantially and significantly decreased in $p53^{-/-}$ cells compared with wildtype cells, supporting the conclusion that the additional effect induced by irradiation requires functional p53 (Supplementary Figure S6).

In $p53^{-/-}$ B16 or A375 melanoma cells, cell-surface calreticulin levels were not further enhanced by combining RIG-I stimulation with irradiation (Figure 5D and E). Correspondingly, irradiation-induced uptake of B16 melanoma cells by DCs was markedly reduced in $p53^{-/-}$ cells compared with wildtype cells. Furthermore, the irradiation-dependent upregulation of the activation markers CD86 and CD69 on DCs upon phagocytosis was not observed in B16 melanoma cells lacking p53 (Figure 5F). These results suggest that the irradiation-dependent effects, including cell death, immunogenicity, subsequent uptake of dying cells by DCs, and activation of DCs, are primarily dependent on the expression of p53 in melanoma cells, whereas the effect of RIG-I stimulation alone is not affected by the absence of p53.

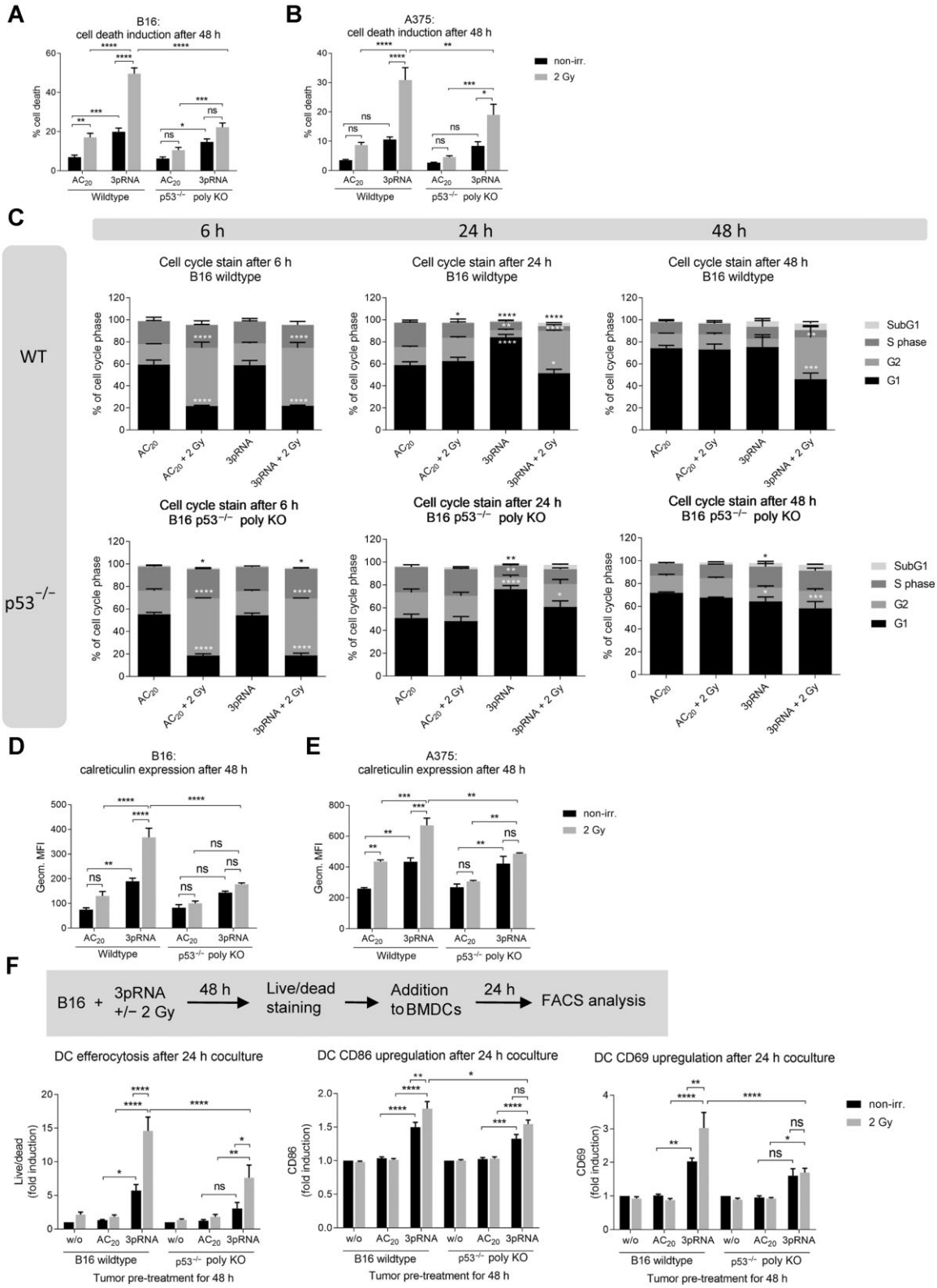

Figure 5 Knocking out p53 reduces the response of melanoma cells to combination treatment. (**A**–**E**) Wildtype or p53$^{-/-}$ B16 or A375 cells were transfected with 50 ng/ml 3pRNA or AC_{20} control RNA, combined with or without 2 Gy irradiation. (**A** and **B**) Induction of cell death was quantitated by Annexin V/7AAD staining and flow cytometry in B16 (**A**) and A375 (**B**) cells. (**C**) Flow-cytometric cell cycle analysis with Hoechst 33342 at the indicated time points in B16 cells. (**D** and **E**) Surface calreticulin expression of B16 (**D**) and A375 (**E**)

Combined antitumour activity of irradiation and RIG-I in vivo depends on functional p53 in melanoma

In the *in vivo* B16 melanoma model, both T cell activation and NK cell activation in the draining lymph nodes were enhanced by 3pRNA injection, as demonstrated by upregulation of CD69 on $CD8^+$ T cells, $CD4^+$ T cells, and $NK1.1^+$ NK cells (Figure 6A; Supplementary Figure S7). The addition of irradiation at the tumour area further enhanced CD69 expression on T cells in the draining lymph nodes of mice injected with wildtype B16 cells, but did not affect that in mice with $p53^{-/-}$ B16 cells (Figure 6A). These findings recapitulated the results of immunogenic cell death and DC activation *in vitro* (Figure 5). Consistently, RIG-I stimulation by 3pRNA significantly reduced tumor growth of both wildtype and $p53^{-/-}$ melanomas, and additional local tumour irradiation further reduced the volume of wildtype tumours but did not significantly affect $p53^{-/-}$ tumours (Figure 6B). However, infiltration of $CD4^+$ T cells, $CD8^+$ T cells, and NK cells in tumour tissues was enhanced by both RIG-I stimulation alone and RIG-I stimulation combined with irradiation, but there was no significant difference between wildtype and $p53^{-/-}$ conditions (Supplementary Figure S8A and B). This might be due to the fact that the most responsive tumours already completely regressed at the time point of evaluation and could not be included in the analysis. The same limitation applies to the measurement of CXCL10 expression in the tumour tissue (Supplementary Figure S8C).

Altogether, our data demonstrate that the effect of combination treatment *in vivo* is dependent on cell-intrinsic p53 expression in tumour cells, whereas the efficacy of RIG-I monotherapy is independent of the p53 status of the tumour.

Discussion

Our results reveal that a combination of RIG-I stimulation with radiotherapy is a highly promising approach for the treatment for tumours with an intact p53 pathway as present in most malignant melanomas (Box et al., 2014). In this study, we demonstrate that localized irradiation of the tumour in a melanoma model substantially improved the therapeutic efficacy of intratumoural injection with RIG-I ligand *in vivo*. This enhanced antitumour effect was accompanied by increased activation of $CD4^+$ and $CD8^+$ T cells in tumour-draining lymph nodes. *In vitro*, low-dose ionizing irradiation of tumour cells synergistically enhanced RIG-I-mediated induction of immunogenic tumour cell death, as characterized by increased cell-surface expression of calreticulin and the release of HMGB1 and inflammatory chemokines and cytokines. The uptake of this immunogenic material activated DCs. Molecularly, the synergistic effect of irradiation and RIG-I depended on the presence of an intact p53 pathway. Enhanced and prolonged activation of p53 (phosphorylation of Ser15) resulted in a prolonged cell cycle arrest of tumour cells in the G2/M phase, which only occurred when RIG-I and irradiation were combined and led to subsequent immunogenic cell death. Notably, the p53 pathway was required for this activity *in vitro* and *in vivo* but not for the antitumour activity of intratumoural injection with RIG-I ligand as a monotherapy. The lack of the combinatorial effect in wildtype mice carrying p53-deficient melanoma provided evidence that a direct tumour cell-intrinsic effect is involved. This is in agreement with the work by Heidegger et al. (2019) who found that optimal efficacy of RIG-I ligand required RIG-I signalling in both tumour cells and the host. Furthermore, in contrast to tumour models using wildtype melanoma cells, $RIG\text{-}I^{-/-}$ melanoma did not show growth reduction when treated with 3pRNA *in vivo* (Engel et al., 2017).

In ~50% of all human tumours, either p53 is mutated or functionally inactive (Olivier et al., 2010) or MDM2 is overexpressed and downregulates p53 expression (Momand et al., 1998). Therefore, our data demonstrating that RIG-I stimulation therapy is independent of p53 are encouraging for RIG-I-mediated immunotherapy in general. Furthermore, based on our results, the combination of RIG-I stimulation with radiotherapy should be limited to tumours with an intact p53 pathway. In melanoma, the frequency of p53 mutations is only 10%–19% (Box et al., 2014), suggesting that the combination therapy is well suited to target malignant melanoma.

Interestingly, there is evidence from previous studies that p53 signalling is important for antiviral defence and IFN signalling (Takaoka et al., 2003; Porta et al., 2005). Moreover, it has been reported that treatment with IFNβ concurrent to irradiation or chemotherapy sensitized mouse embryonic fibroblasts and human hepatic cancer cells for a higher induction of apoptosis (Takaoka et al., 2003). However, in our study, recombinant type I IFN was not a sufficient substitute for RIG-I stimulation, since it did not trigger the enhanced and prolonged p53 phosphorylation or immunogenic cell death by radiotherapy.

Upregulation of p53 by RIG-I in our study is in agreement with findings reported in the recent literature. Zhang et al. (2020) have demonstrated that mitochondrial antiviral signalling protein (MAVS, downstream signalling molecule of RIG-I) is a key regulator of p53 activation. They found that MAVS promotes p53-dependent cell death in response to DNA damage (etoposide and deferoxamine) by stabilization of p53 via inhibition of p53 ubiquitination. However, the combination with irradiation has not been examined in their study.

To date, two studies have examined the combination of poly(I:C) with irradiation (Yoshino et al., 2018; Domankevich et al., 2020). However, it should be noted that poly(I:C) activates multiple dsRNA receptors, including protein

Figure 5 *(Continued)* cells was monitored at 48 h after treatment by flow cytometry. (**F**) Wildtype or $p53^{-/-}$ B16 cells were transfected with 200 ng/ml 3pRNA and irradiated (2 Gy) as indicated. After 48 h, cells were stained by eFluor780 dye and cocultured with BMDCs overnight. Activated DCs were analyzed by flow cytometry on the next day. All data are shown as mean ± SEM of $n = 10$ (**A**), $n = 5$ (**D**), or $n = 3$ (**B**, **C**, **E**, and **F**). *$P < 0.05$; **$P < 0.01$; ***$P < 0.001$; ****$P < 0.0001$; two-way ANOVA. geom. MFI, geometric mean fluorescence intensity; ns, not significant; w/o, untreated; non-irr., non-irradiated.

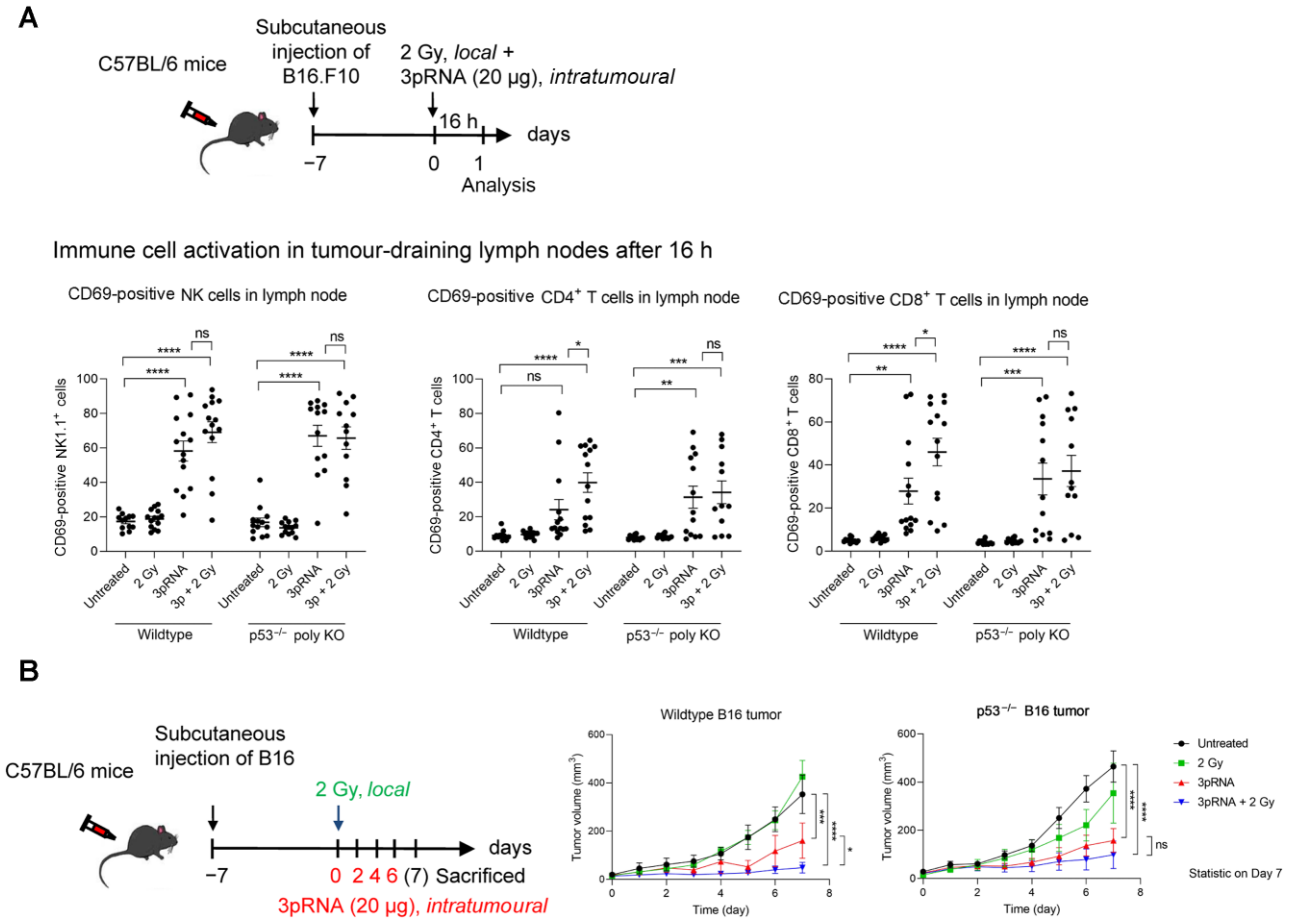

Figure 6 Synergistic antitumour activity of irradiation and RIG-I activation *in vivo* depends on functional p53 in melanoma. (**A**) Wildtype or $p53^{-/-}$ B16 cells were subcutaneously transplanted into C57/BL6 mice. The mice were then locally irradiated (2 Gy), injected with 20 µg 3pRNA, or treated by both. After 16 h, the mice were sacrificed. Tumour-draining lymph nodes were analyzed by flow cytometry for CD69 surface expression of activated $CD8^+$ T cells, $CD4^+$ T cells, and $NK1.1^+$ NK cells. Mean ± SEM of $n = 3$ with 3–5 mice per group and experiment. (**B**) Mice were treated as indicated over 7 days and the tumour size was measured daily. Mean ± SEM of $n = 3$ with 3–5 mice per group and experiment. ns, not significant; *$P < 0.05$; **$P < 0.01$; ***$P < 0.001$; ****$P < 0.0001$; two-way ANOVA.

kinase R, 2′-5′-oligoadenylate synthetase (OAS), Z-DNA-binding protein 1, toll-like receptor 3, melanoma differentiation-associated protein 5, and RIG-I (Bartok and Hartmann, 2020), rendering this rather nonspecific immunotherapeutic approach more prone to interindividual variability and immunotoxic side effects. In one study, the combination of irradiation and poly(I:C) activation was studied in lung carcinoma cell lines, where the cotreatment (with 4 Gy irradiation) was demonstrated to enhance the cytotoxic effects of both monotherapies in a caspase-dependent manner *in vitro* (Yoshino et al., 2018), but no *in vivo* data were presented in their work. Another study has demonstrated synergistic inhibition of tumour growth and enhanced induction of long-term immune memory cells in murine mammary and pancreatic carcinoma models using a combination of poly(I:C) injection with transplantation of α-emitting radiation seeds into the tumour (Domankevich et al., 2020), an experimental treatment that is currently being tested in clinical trials. However, irradiation with a clinical linear accelerator, as used in our study, rather than α-emitting radiation seeds, is a well-established treatment method for cancer patients.

Another interesting aspect of irradiation and immunity is that, localized irradiation by itself, independent of additional innate immune activation, has been shown to improve tumour infiltration of adoptively transferred T cells in a pancreatic cancer model (Klug et al., 2013). With regard to irradiation intensity, other studies have shown that low doses (2–8 Gy) of irradiation elicit stronger antitumour immunity compared with higher doses, especially when given repetitively or combined with other antitumoural treatments (Gameiro et al., 2014; Vanpouille-Box et al., 2017; Chen et al., 2020). In our study, despite the modest antitumoural response was induced by 2 Gy irradiation alone, this low dose turned out to be more advantageous at coactivating RIG-I-mediated immunity than the higher doses (5 or 10 Gy).

Monotherapy with RIG-I agonists has been reported in several studies, demonstrating that intratumoural injection of RIG-I ligands induces an effective antitumour immune response

(Poeck et al., 2008; Heidegger et al., 2019). Importantly, our results highlight that not only RIG-I activation has the potential to improve the efficacy of conventional radiotherapy, but also RIG-I therapy itself can be improved by adding low-dose irradiation. According to our data, the combination with low-dose irradiation may enable a reduction in the required dose of RIG-I agonist to achieve effective treatment. To date, RIG-I agonist monotherapy has remained technically challenging and is limited by the injection volumes and RNA concentrations that can be achieved through the current delivery systems (Whitehead et al., 2009). Thus, if the combination therapy requires a reduced amount of RIG-I ligand, it could improve the feasibility of RIG-I agonist treatment.

Other therapeutic agents that enhance RIG-I expression or activation may be useful to overcome radioresistance of p53-expressing tumours such as melanoma. For example, it has been reported that DNA methylation inhibitors such as 5-AZA and Decitabine induce endogenous dsRNA in the context of demethylation of endogenous retroviral elements, thereby inducing RIG-I-like receptor expression and activating downstream signalling (Chiappinelli et al., 2015; Roulois et al., 2015). However, in our experiments, melanoma cell death induction by both 5-AZA and Decitabine was not further enhanced by irradiation. Neither 5-AZA nor Decitabine consistently upregulated RIG-I expression in our experimental system. This could be due to a much lower RIG-I-stimulatory activity of DNA methylation inhibitors compared with a potent specific RIG-I ligand used in this study. Furthermore, a prolonged exposure of tumour cells to DNA methylation inhibitors might be necessary to cause considerable RIG-I activation. Another aspect is that long dsRNA induced by DNA methylation inhibitors has been shown to induce other dsRNA-dependent pathways such as the OAS–RNase L pathway (Banerjee et al., 2019) to add complexity.

Since RIG-I was originally identified as a gene induced by retinoic acid in a promyelocytic leukaemia cell line (Sun, 1997), ATRA represents another candidate for combination with irradiation. However, the induction of RIG-I expression in melanoma cells by ATRA is magnitudes lower than that by a RIG-I ligand (Szabo et al., 2016), and thus it is not surprising that, in our study, upregulation of RIG-I expression with ATRA was marginal, and irradiation resistance of B16 melanoma cells was not improved by exposure to ATRA. Based on our results, it will be interesting to explore the combination of RIG-I immunotherapy with other genotoxic agents, such as Cisplatin, or with p53 agonists, such as the MDM2 inhibitor APG-115.

Altogether, our study clearly demonstrates that the combination of DNA-damaging radiotherapy with innate-immune stimulating RIG-I ligand synergistically boosts p53-dependent immunogenic tumour cell death, underscoring the rationale for evaluating a localized combination therapy that turns cold into hot tumours as an *in situ* cancer vaccine (van den Boorn and Hartmann, 2013). Since melanoma is classically considered a 'radioresistant' tumour, our study also provides a new rationale for re-evaluating radiotherapy in combination with RIG-I activation for a broad range of cancers. Moreover, combining with other synergistic treatments, the individual radiation doses can be reduced, which may reduce the severe side effects associated with standard radiotherapy.

Materials and methods

Cell lines

Human A375 and SKmel28 melanoma cells, A549 lung adenocarcinoma cells, and murine B16.F10 melanoma cells were cultured in DMEM, and human MaMel19, MaMel54, and MaMel48 melanoma cells were cultured in RPMI 1640, both media supplemented with 10% foetal bovine serum (FBS), 100 IU/ml penicillin, and 100 µg/ml streptomycin (all from Thermo Fisher Scientific), in a humidified incubator at 37°C and 5% CO_2. A375 cells were kindly provided by Michael Hölzel (University Hospital Bonn, Germany), and MaMel19, MaMel54, and MaMel48 cells were kindly provided by Jennifer Landsberg (University Hospital Bonn, Germany) and Dirk Schadendorf (University Hospital Essen, Germany). B16 and Skmel28 cells were purchased from ATCC. The identity of the human cell lines was confirmed by short-tandem-repeat profiling (Eurofins). Cells were checked monthly for mycoplasma infection.

Oligonucleotides, reagents, and chemicals

3pRNA was *in vitro* transcribed from a DNA template by using the phage T7 polymerase from the Transcript Aid T7 High Yield Transcription Kit (Fermentas), as described previously (Goldeck et al., 2014). Inert AC_{20} control RNA (5′-CACAACAAACCAAACAACCA-3′) and polyA RNA were obtained from Biomers and Sigma–Aldrich, respectively. Murine IFNα was purchased from BioLegend. The MDM2 inhibitor AMG232 was purchased from MedChemExpress. 5-AZA, Decitabine, and ATRA were all purchased from MedChemExpress, dissolved in dimethyl sulfoxide and diluted in cell culture medium for the treatment of B16 melanoma cells.

Oligonucleotide transfection of tumour cells

Lipofectamine 2000 (Invitrogen) and OptiMem (Thermo Fisher Scientific) were used according to the manufacturer's protocol to transfect control AC_{20} RNA or stimulatory 3pRNA at the indicated concentrations.

Irradiation of tumour cells

Cells were irradiated with high-energy photons (150 keV) generated by a biological irradiator (RS-2000, Rad Source Technologies) at 30 min after transfection of RNA or stimulation with IFNα.

Uptake of melanoma cells by DCs

BMDCs were generated from wildtype C57BL/6 mice as described previously (Gehrke et al., 2013). B16 melanoma cells were stimulated as indicated in the figures. After 48 h, melanoma cells were stained with eFluor780 fixable viability dye (eBioscience, 1:2000 in phosphate-buffered saline (PBS)) for

30 min on ice. Excess dye was washed away by the addition of 200 µl DMEM supplemented with 10% FBS. Stained melanoma cells (25000) were then cocultured in a 96-well plate with 100000 BMDCs overnight. On the next day, DCs were detached by adding 2 mM EDTA/PBS and analyzed by flow cytometry.

Generation of polyclonal p53-knockout cell lines by using CRISPR/Cas9

The CRISPR target site for murine p53 (single guide (sg) RNA: 5′-CTGAGCCAGGAGACATTTTC-3′) was cloned into a px330 plasmid (px330-U6-Chimeric_BB-CBh-hSpCas9, Addgene plasmid #42230) and the site for human p53 (sgRNA: 5′-GCATCTTATCCGAGTGGA-3′) was cloned into a px459 plasmid (pSpCas9(BB)-2A-Puro (px459) V2.0, Addgene plasmid #62988), both kindly provided by Daniel Hinze from the lab of Michael Hölzel. B16 and A375 cells were seeded at a density of 5×10^4 cells per well into a 12-well plate on the day before the transfection with 2 µg of the CRISPR/Cas9 plasmid using Lipofectamine 2000. After 3 days of incubation at 37°C, the transfected cells were seeded out again into 12-well plates at a density of 5×10^3 cells per well. One day later, 10 µM of the MDM2 inhibitor AMG232 was added to the culture medium for five days to positively select p53-deficient cells.

Gene-expression analysis with microarray

B16.F10 cells were transfected with 50 ng/ml 3pRNA or AC_{20} control RNA and either irradiated (2 Gy) or not for 6 h. RNA was isolated with the RNeasy Mini Kit (Qiagen), according to the manufacturer's instructions. The extracted RNA was further processed using a Clariom S Mouse Genechip (Thermo Fisher) at the LIFE & BRAIN Genomics Service Centre, Bonn.

Western blot analysis

Total cellular protein was extracted as described previously (Engel et al., 2017). Then, 30–50 µg of protein was mixed with an equal amount of 2× Laemmli buffer (200 mM Tris–HCl, pH 6.8, 4% sodium dodecyl sulfate (SDS), 20% glycerol, and 200 mM DTT), denatured at 95°C for 5 min, separated by SDS gel electrophoresis (30 mA per gel, 1.5 h), and transferred onto a nitrocellulose membrane (GE Healthcare, 0.45-µm pore size) using 450 mA for 1.5 h. The membranes were blocked with 5% non-fat dry milk in TBST buffer (150 mM NaCl, 20 mM Tris, 0.1% Tween 20, pH 7.6) for 1 h at room temperature (RT), incubated with the respective primary antibodies (anti-phospho-p53 (Ser15), anti-p53, anti-PUMA, and anti-p21 (all 1:1000, Cell Signaling Technology)) at 4°C overnight, and then incubated with HRP-coupled secondary antibodies (1:5000, Cell Signaling Technology) or IRDye800-coupled anti-rabbit and anti-mouse antibodies (1:10000, LI-COR Biosciences) in 5% milk/TBST for 1 h at RT. Anti-actin-HRP antibody (1:5000, Santa Cruz) or mouse/rabbit anti-β-actin (1:10000, LI-COR Biosciences) was used to detect actin as a loading control. Protein bands were detected by chemiluminescence of the ECL Western Blotting Substrate (Thermo Scientific) or by near-infrared fluorescence with the Odyssey Fc (LI-COR Biosciences).

ELISA

HMGB1 ELISA kit from IBL International was used according to the manufacturer's protocol.

Flow cytometry

Cells of interest were harvested with trypsin and washed with PBS. For staining of surface proteins, fluorochrome-conjugated monoclonal antibodies were diluted 1:200 in FACS buffer (1× PBS containing 10% FBS, 2 mM EDTA, and 0.05% sodium azide) and incubated with the cells for 15–20 min on ice or RT. Antibodies used were: APC-Cy7 or BV510 anti-CD4, PerCP-Cy5.5 or BV421 anti-CD8, PerCP anti-CD45, BV421 anti-CD11c, Alexa-Fluor-488 or BV510 anti-CD69, BV785 anti-CD86, BV785 or BV510 anti-MHC-I (Hk2b), FITC anti-I-A/E (all BioLegend), FITC anti-CD11c, APC anti-MHC-I (Hk2b), PE or BV650 anti-NK1.1 (all eBioscience), BUV737 anti-CD4, BUV395 anti-CD8, BUV395 anti-CD11b, FITC anti-HLA ABC (all BD Bioscience), and Alexa-488 anti-Calreticulin (Cell Signaling Technology, diluted 1:100).

For *in vivo* studies, the tissue was digested with 1 mg/ml collagenase D in PBS with 5% FBS for 20 min at 37°C and afterwards passed through a 70-µm cell strainer with PBS. Cells were stained with Zombie UV fixable viability stain (1:500 in PBS, BioLegend) for 20 min at RT, followed by blocking of Fc receptors (anti-mouse CD16/32 from eBioscience, 1:200 in FACS buffer) for 15 min on ice. Surface staining was performed as described above.

Intracellular staining of activated, cleaved caspase 3 was analyzed using a rabbit anti-cleaved caspase 3 monoclonal antibody (1:500, Cell Signaling Technology) followed by a second staining with FITC-anti-rabbit IgG (1:200, BioLegend). Both antibodies were diluted in FACS buffer supplemented with 0.5% saponin.

Fluorescence intensities for all of the flow-cytometry-based assays were measured with the LSRFortessa flow cytometer (BD Biosciences) or with the Attune NxT Flow Cytometer (Thermo Fisher).

Quantification of apoptotic cell death

Cells were stained with Annexin V-Alexa 647 or Annexin V-Pacific Blue (both 1:30, BioLegend) in Annexin binding buffer (10 mM HEPES, pH 7.4, 140 mM NaCl, 2.5 mM $CaCl_2$) and incubated at RT for 20 min in the dark. Cells were washed and resuspended in 200 µl 1× binding buffer. Then, 5 µl of 7AAD working solution (50 µg/ml in PBS, Thermo Fisher Scientific) was added to the stained cells at 5–10 min before measurement.

Multiplex cytokine assay

Cytokine levels were measured using human and mouse LEGENDplex bead-based multi-analyte flow assay kits, following the manufacturer's manual, except that the assay was performed in a 384-well plate and the volumes were adjusted accordingly.

Cell cycle analysis

Analysis of cell cycle phases was performed in cells fixed and permeabilized with 70% ethanol for 1 h at RT. Cells were incubated for 30 min at RT with 10 µg/ml propidium iodide and 100 µg/ml RNase A in FACS buffer, and then directly analyzed by flow cytometry. For simultaneous staining of activated caspase 3, the cultivation medium of cells seeded in 96-well plates was exchanged for 50 µl/well of staining solution, containing CellEvent Caspase3/7 Green ReadyProbes, according to the manufacturer's protocol, and 100 µg/ml Hoechst 33342 (both Thermo Fisher Scientific) and incubated for 30–60 min at 37°C. The cells were then detached and analyzed by flow cytometry.

In vivo studies with mice

The 8–12-week-old female C57BL/6 mice were obtained from Janvier and housed in individually ventilated cages in the House of Experimental Therapy at the University Hospital Bonn under specific-pathogen-free conditions. Sample size was calculated *a priori* with G*Power (Faul et al., 2007). All experiments were approved by the animal ethics committee. After at least 3 days of acclimatization, mice were injected subcutaneously into the right flank of the back with 1×10^5 B16.F10 cells in 100 µl sterile PBS. Mice without tumour at the start of the experiment and mice with a tumour >4 mm in diameter at the start of a survival or tumour-size experiment were excluded. When the tumours reached a diameter of 3–4 mm, they were injected with 20 µg 3pRNA or control RNA complexed with *in vivo*-jetPEI (Polyplus) according to the manufacturer's protocol and afterwards locally irradiated with a single dose of 2 Gy. For local irradiation, the mice were narcotized and positioned in the treatment beam. The tumours were stereotactically irradiated with adapted field size in a range of 1–2 cm using a linear accelerator with a 6 MeV beam (TrueBeam STx, Varian and Mevatron MD, Siemens). The mice were surrounded by water-equivalent RW3 sheets (PTW) and placed in the depth-plane Dmax (15 mm) of the 6 MeV beam. The tumour size was measured daily with a caliper and the volume was calculated with the formula $V = (W^2 \times L)/2$. For the survival studies, mice with tumours >10 mm in diameter had to be euthanized for ethical reasons.

Ethics approval and consent to participate

All animal experiments were approved by the local authorities (LANUV NRW).

Statistical analysis

If not indicated otherwise, data are presented as mean ± SEM of at least three experiments. Normal distribution of the data was tested with the Shapiro–Wilk test. A statistical analysis of the difference between groups using *t*-test, one or two-way ANOVA, or Kruskal–Wallis test as appropriate and stated in the figure legends, was calculated with GraphPad Prism 9. *$P < 0.05$; **$P < 0.01$; ***$P < 0.001$; ****$P < 0.0001$; ns, not significant.

Supplementary material

Supplementary material is available at *Journal of Molecular Cell Biology* online.

Acknowledgements

We thank Meghan Lucas for her critical reading of this manuscript. We thank Daniel Hinze (University Hospital Bonn) for providing us with CRISPR gRNA/Cas9 plasmids targeting p53. We thank Jennifer Landsberg (University Hospital Bonn) for her helpful scientific discussions.

Funding

This study was funded by Deutsche Forschungsgemeinschaft (DFG, German Research Foundation) under Germany's Excellence Strategy EXC2151 390873048 of which E.B., G.H., and M.S. are members. It was also supported by other grants of DFG, including Project-ID 369799452 TRR237 to E.B., G.H., and M.S., Project-ID 397484323 TRR259 to G.H., GRK 2168 to E.B. and M.S., and DFG SCHL1930/1-2. M.R. was funded by the Deutsche Krebshilfe through a Mildred Scheel Nachwuchszentrum (70113307). S.L. was the recipient of a PhD scholarship from Bayer Pharma AG (40860128).

Conflict of interest: M.S., J.G.v.d.B., and G.H. are inventors on a patent covering synthetic RIG-I ligand. M.R. and G.H. were cofounders of Rigontec GmbH.

References

Apetoh, L., Ghiringhelli, F., Tesniere, A., et al. (2007). Toll-like receptor 4-dependent contribution of the immune system to anticancer chemotherapy and radiotherapy. Nat. Med. *13*, 1050–1059.

Banerjee, S., Gusho, E., Gaughan, C., et al. (2019). OAS-RNase L innate immune pathway mediates the cytotoxicity of a DNA-demethylating drug. Proc. Natl Acad. Sci. USA *116*, 5071–5076.

Bartok, E., and Hartmann, G. (2020). Immune sensing mechanisms that discriminate self from altered self and foreign nucleic acids. Immunity *53*, 54–77.

Bek, S., Stritzke, F., Wintges, A., et al. (2019). Targeting intrinsic RIG-I signaling turns melanoma cells into type I interferon-releasing cellular antitumor vaccines. Oncoimmunology *8*, e1570779.

Besch, R., Poeck, H., Hohenauer, T., et al. (2009). Proapoptotic signaling induced by RIG-I and MDA-5 results in type I interferon-independent apoptosis in human melanoma cells. J. Clin. Invest. *119*, 2399–2411.

Bonaventura, P., Shekarian, T., Alcazer, V., et al. (2019). Cold tumors: a therapeutic challenge for immunotherapy. Front. Immunol. *10*, 168.

Box, N.F., Vukmer, T.O., and Terzian, T. (2014). Targeting p53 in melanoma. Pigment Cell Melanoma Res. *27*, 8–10.

Castiello, L., Zevini, A., Vulpis, E., et al. (2019). An optimized retinoic acid-inducible gene I agonist M8 induces immunogenic cell death markers in human cancer cells and dendritic cell activation. Cancer Immunol. Immunother. *68*, 1479–1492.

Chen, J., Harding, S.M., Natesan, R., et al. (2020). Cell cycle checkpoints cooperate to suppress DNA- and RNA-associated molecular pattern recognition and anti-tumor immune responses. Cell Rep. *32*, 108080.

Chiappinelli, K.B., et al. (2015). Inhibiting DNA methylation causes an interferon response in cancer via dsRNA including endogenous retroviruses. Cell *162*, 974–986.

Delaney, G.P., and Barton, M.B. (2015). Evidence-based estimates of the demand for radiotherapy. Clin. Oncol. *27*, 70–76.

Domankevich, V., Efrati, M., Schmidt, M., et al. (2020). RIG-1-like receptor activation synergizes with intratumoral alpha radiation to induce pancreatic tumor rejection, triple-negative breast metastases clearance, and antitumor immune memory in mice. Front. Oncol. *10*, 990.

Duewell, P., Steger, A., Lohr, H., et al. (2014). RIG-I-like helicases induce immunogenic cell death of pancreatic cancer cells and sensitize tumors toward killing by $CD8^+$ T cells. Cell Death Differ. *21*, 1825–1837.

Engel, C., Brugmann, G., Lambing, S., et al. (2017). RIG-I resists hypoxia-induced immunosuppression and dedifferentiation. Cancer Immunol. Res. *5*, 455–467.

Esfahani, K., Roudaia, L., Buhlaiga, N., et al. (2020). A review of cancer immunotherapy: from the past, to the present, to the future. Curr. Oncol. *27*, S87–S97.

Faul, F., Erdfelder, E., Lang, A.G., et al. (2007). G*Power 3: a flexible statistical power analysis program for the social, behavioral, and biomedical sciences. Behav. Res. Methods *39*, 175–191.

Gameiro, S.R., Jammeh, M.L., Wattenberg, M.M., et al. (2014). Radiation-induced immunogenic modulation of tumor enhances antigen processing and calreticulin exposure, resulting in enhanced T-cell killing. Oncotarget *5*, 403–416.

Gehrke, N., Mertens, C., Zillinger, T., et al. (2013). Oxidative damage of DNA confers resistance to cytosolic nuclease TREX1 degradation and potentiates STING-dependent immune sensing. Immunity *39*, 482–495.

Goldeck, M., Schlee, M., Hartmann, G., et al. (2014). Enzymatic synthesis and purification of a defined RIG-I ligand. Methods Mol. Biol. *1169*, 15–25.

Golden, E.B., Frances, D., Pellicciotta, I., et al. (2014). Radiation fosters dose-dependent and chemotherapy-induced immunogenic cell death. Oncoimmunology *3*, e28518.

Goubau, D., Schlee, M., Deddouche, S., et al. (2014). Antiviral immunity via RIG-I-mediated recognition of RNA bearing 5′-diphosphates. Nature *514*, 372–375.

Hallahan, D.E., Spriggs, D.R., Beckett, M.A., et al. (1989). Increased tumor necrosis factor alpha mRNA after cellular exposure to ionizing radiation. Proc. Natl Acad. Sci. USA *86*, 10104–10107.

Haluska, F.G., Tsao, H., Wu, H., et al. (2006). Genetic alterations in signaling pathways in melanoma. Clin. Cancer Res. *12*, 2301s–2307s.

Hauser, S.H., Calorini, L., Wazer, D.E., et al. (1993). Radiation-enhanced expression of major histocompatibility complex class I antigen H-2Db in B16 melanoma cells. Cancer Res. *53*, 1952–1955.

Heidegger, S., Kreppel, D., Bscheider, M., et al. (2019). RIG-I activating immunostimulatory RNA boosts the efficacy of anticancer vaccines and synergizes with immune checkpoint blockade. EBioMedicine *41*, 146–155.

Hornung, V., Ellegast, J., Kim, S., et al. (2006). 5′-Triphosphate RNA is the ligand for RIG-I. Science *314*, 994–997.

Kang, J., Demaria, S., and Formenti, S. (2016). Current clinical trials testing the combination of immunotherapy with radiotherapy. J. Immunother. Cancer *4*, 51.

Klug, F., Prakash, H., Huber, P.E., et al. (2013). Low-dose irradiation programs macrophage differentiation to an $iNOS^+$/M1 phenotype that orchestrates effective T cell immunotherapy. Cancer Cell *24*, 589–602.

Lee, Y., Auh, S.L., Wang, Y., et al. (2009). Therapeutic effects of ablative radiation on local tumor require $CD8^+$ T cells: changing strategies for cancer treatment. Blood *114*, 589–595.

Mahadevan, A., Patel, V.L., and Dagoglu, N. (2015). Radiation therapy in the management of malignant melanoma. Oncology *29*, 743–751.

Marcus, A., Mao, A.J., Lensink-Vasan, M., et al. (2018). Tumor-derived cGAMP triggers a STING-mediated interferon response in non-tumor cells to activate the NK cell response. Immunity *49*, 754–763.e4.

Matsumura, S., Wang, B., Kawashima, N., et al. (2008). Radiation-induced CXCL16 release by breast cancer cells attracts effector T cells. J. Immunol. *181*, 3099–3107.

Momand, J., Jung, D., Wilczynski, S., et al. (1998). The MDM2 gene amplification database. Nucleic Acids Res. *26*, 3453–3459.

Obeid, M., Panaretakis, T., Joza, N., et al. (2007). Calreticulin exposure is required for the immunogenicity of gamma-irradiation and UVC light-induced apoptosis. Cell Death Different. *14*, 1848–1850.

Obeid, M., Tesniere, A., Ghiringhelli, F., et al. (2007b). Calreticulin exposure dictates the immunogenicity of cancer cell death. Nat. Med. *13*, 54–61.

Ohshima, Y., Tsukimoto, M., Takenouchi, T., et al. (2010). γ-Irradiation induces $P2X_7$ receptor-dependent ATP release from B16 melanoma cells. Biochim. Biophys. Acta *1800*, 40–46.

Olivier, M., Hollstein, M., and Hainaut, P. (2010). TP53 mutations in human cancers: origins, consequences, and clinical use. Cold Spring Harb. Perspect. Biol. *2*, a001008.

Poeck, H., Besch, R., Maihoefer, C., et al. (2008). 5′-Triphosphate-siRNA: turning gene silencing and Rig-I activation against melanoma. Nat. Med. *14*, 1256–1263.

Porta, C., Hadj-Slimane, R., Nejmeddine, M., et al. (2005). Interferons α and γ induce p53-dependent and p53-independent apoptosis, respectively. Oncogene *24*, 605–615.

Reits, E.A., Hodge, J.W., Herberts, C.A., et al. (2006). Radiation modulates the peptide repertoire, enhances MHC class I expression, and induces successful antitumor immunotherapy. J. Exp. Med. *203*, 1259–1271.

Roulois, D., Yau, H.L., Singhania, R., et al. (2015). DNA-demethylating agents target colorectal cancer cells by inducing viral mimicry by endogenous transcripts. Cell *162*, 961–973.

Schadt, L., Sparano, C., Schweiger, N.A., et al. (2019). Cancer-cell-intrinsic cGAS expression mediates tumor immunogenicity. Cell Rep. *29*, 1236–1248.e7.

Schlee, M., Roth, A., Hornung, V., et al. (2009). Recognition of 5′ triphosphate by RIG-I helicase requires short blunt double-stranded RNA as contained in panhandle of negative-strand virus. Immunity *31*, 25–34.

Sun, Y.W. (1997). Rig-I, a homolog gene of RNA helicase, is induced by retinoic acid during the differentiation of acute promyelocytic leukemia cell. Thesis. Shanhai Institute of Hematology, Rui Jin Hospital, Shanghai Second Medical University.

Szabo, A., Fekete, T., Koncz, G., et al. (2016). RIG-I inhibits the MAPK-dependent proliferation of BRAF mutant melanoma cells via MKP-1. Cell. Signal. *28*, 335–347.

Takaoka, A., Hayakawa, S., Yanai, H., et al. (2003). Integration of interferon-α/β signalling to p53 responses in tumour suppression and antiviral defence. Nature *424*, 516–523.

van den Berg, J., Castricum, K.C.M., Meel, M.H., et al. (2020). Development of transient radioresistance during fractionated irradiation in vitro. Radiother. Oncol. *148*, 107–114.

van den Boorn, J.G., and Hartmann, G. (2013). Turning tumors into vaccines: co-opting the innate immune system. Immunity *39*, 27–37.

Vanpouille-Box, C., Alard, A., Aryankalayil, M.J., et al. (2017). DNA exonuclease Trex1 regulates radiotherapy-induced tumour immunogenicity. Nat. Commun. *8*, 15618.

Whitehead, K.A., Langer, R., and Anderson, D.G. (2009). Knocking down barriers: advances in siRNA delivery. Nat. Rev. Drug Discov. *8*, 129–138.

Yoshino, H., Iwabuchi, M., Kazama, Y., et al. (2018). Effects of retinoic acid-inducible gene-I-like receptors activations and ionizing radiation cotreatment on cytotoxicity against human non-small cell lung cancer in vitro. Oncol. Lett. *15*, 4697–4705.

Zhang, W., Gong, J., Yang, H., et al. (2020). The mitochondrial protein MAVS stabilizes p53 to suppress tumorigenesis. Cell Rep. *30*, 725–738.e4.

Received March 13, 2022. Revised September 25, 2022. Accepted January 9, 2023.